ACS APPLIED MATERIALS & INTERFACES

Research Article

www.acsami.org

One-Step Electrodeposition Process To Fabricate Corrosion-Resistant Superhydrophobic Surface on Magnesium Alloy

Qin Liu, Dexin Chen, and Zhixin Kang*

School of Mechanical and Automotive Engineering, South China University of Technology, Guangzhou 510640, China

ABSTRACT: A simple, one-step method has been developed to construct a superhydrophobic surface by electrodepositing Mg−Mn−Ce magnesium plate in an ethanol solution containing cerium nitrate hexahydrate and myristic acid. Scanning electron microscopy, energy-dispersive X-ray spectroscopy, X-ray photoelectron spectroscopy, and Fourier transform infrared spectroscopy were employed to characterize the surfaces. The shortest electrodeposition time to obtain a superhydrophobic surface was about 1 min, and the as-prepared superhydrophobic surfaces had a maximum contact angle of 159.8° and a sliding angle of less than 2°. Potentiodynamic polarization and electrochemical impedance spectroscopy measurements demonstrated that the superhydrophobic surface greatly improved the corrosion properties of magnesium alloy in 3.5 wt % aqueous solutions of NaCl, Na_2SO_4, $NaClO_3$, and $NaNO_3$. Besides, the chemical stability and mechanical durability of the as-prepared superhydrophobic surface were also examined. The presented method is rapid, low-cost, and environmentally friendly and thus should be of significant value for the industrial fabrication of anticorrosive superhydrophobic surfaces and should have a promising future in expanding the applications of magnesium alloys.

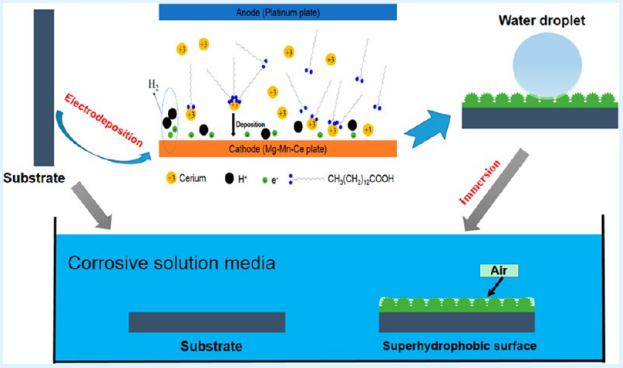

KEYWORDS: *one-step, superhydrophobic, magnesium, electrodeposition, hierarchical structure, corrosion*

1. INTRODUCTION

Metal corrosion due to the interaction of the metal and its environment causes a tremendous economic loss each year.[1] Unfortunately, corrosion cannot be prevented, and therefore, decreasing the corrosion rate has attracted much attention, with research focused on slowing the kinetics and/or altering its mechanism.[2] To date, methods to control corrosion of metals mainly include cathodic protection, fabrication of protective coatings, use of corrosion inhibitors, or combinations of the above methods. Inspired by the self-cleaning lotus leaf and "anti-water" leg of a water stride, the use of superhydrophobic surfaces with water contact angles larger than 150° and sliding angles smaller than 10° has been considered as one of the promising methods to improve metals' corrosion performance because they could inhibit the contact of a surface with water and environmental humidity.[3−5]

Among various metals and their alloys, magnesium and its alloys as the lightest engineering metal materials have attracted considerable interest in the aerospace and electronic industries for their excellent properties, such as low density, high ductility, high specific strength, and electromagnetic compatibility.[6−8] Nevertheless, magnesium is a very active metal and easily corrodes in aqueous solution or a humid atmosphere, which seriously prevents the large-scale application of Mg alloys.[9,10] Herein, the preparation of superhydrophobic surfaces is considered as a promising method to improve the corrosion performance of magnesium and its alloys.[11−13]

In recent years, various methods have been explored to fabricate superhydrophobic surfaces on magnesium alloys, such as hydrothermal synthesis,[11] chemical vapor deposition,[14] chemical etching,[15] microarc oxidation,[16] anodic oxidation,[17] electrochemical deposition,[18] etc. For example, in 2008 Jiang reported a facial chemical etching method to fabricate a superhydrophobic Mg−Li alloy surface.[19] In 2010, Ishizaki fabricated a superhydrophobic surface on AZ31 alloy via microwave plasma-enhanced chemical vapor deposition.[14] In 2012, Li prepared a superhydrophobic surface on AZ91D alloy via electroless plating of nickel and electrodeposition of copper followed by modification with lauric acid.[20] In 2014, Wang fabricated a superhydrophobic surface on AZ31 alloy via a hydrothermal synthesis method followed by modification with fluoroalkylsilane (FAS).[11] However, most of the mentioned methods usually require special conditions, expensive materials, and complex multistep processing procedures, limiting their practical applications. Furthermore, many methods involve the use of biological poison materials, such as FAS, to achieve a low-energy surface.

Currently, electrodeposition has emerged as a competitive technique to fabricate superhydrophobic surfaces because of its advantages such as easy control, simplicity, low cost, and ability

Received: October 31, 2014
Accepted: January 5, 2015
Published: January 5, 2015

DOI: 10.1021/am507586u
ACS Appl. Mater. Interfaces 2015, 7, 1859−1867

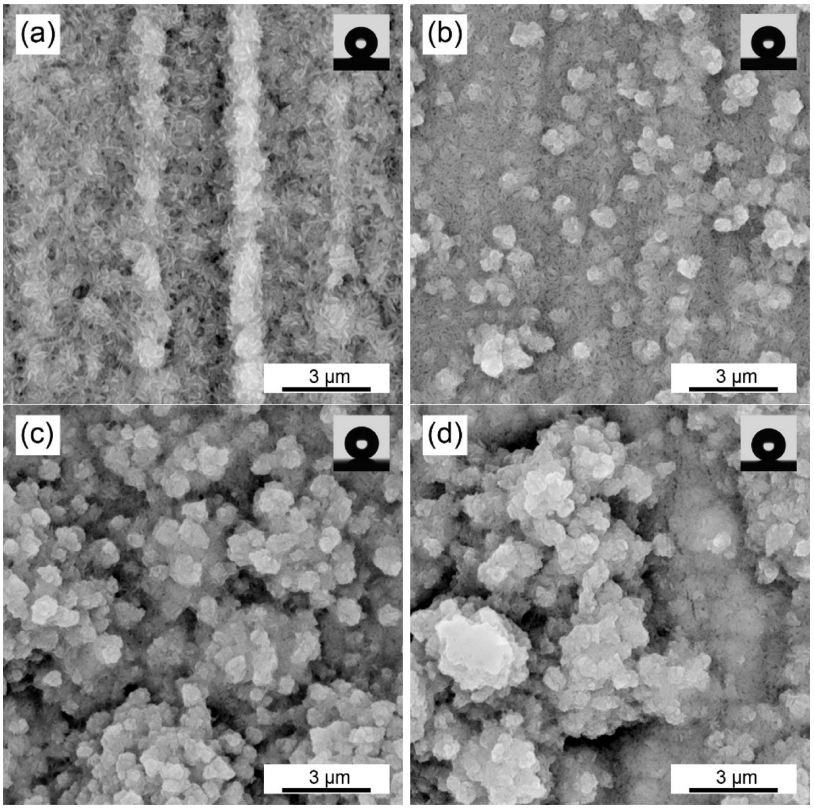

Figure 1. SEM images and (insets) water contact angles of the as-prepared superhydrophobic surfaces obtained at different electrodeposition voltages: (a) 10 V, (b) 20 V, (c) 30 V, and (d) 40 V.

to make large-area surfaces.[17,20,21] Although a few papers have reported the electrodeposition of superhydrophobic surfaces on magnesium alloys, they all require the preparation of a transition-metal layer such as a nickel or zinc film to fabricate a rough structure, which is followed by modification with the low-surface-energy material.[22−24] Moreover, the pretreatment procedure to prepare the transition-metal layer is complicated. Generally, the way to fabricate a superhydrophobic surface involves two steps: the first step is to form a surface with a micro/nanostructured roughness and then to modify that surface using low-surface-energy substances. If both processes can be done in just one step, the process of preparing superhydrophobic surfaces would be simplified and the fabrication time would be shorted. To the best of our knowledge, a rapid one-step electrodeposition method to create a corrosion-resistant superhydrophobic surface based on magnesium and its alloys has rarely been reported.

In this paper, a simple, environmentally friendly one-step electrodeposition method to fabricate a superhydrophobic surface on Mg−Mn−Ce magnesium alloy is presented. The coating with a micro/nanorough structure and a high contact angle produces a Mg−Mn−Ce magnesium alloy with desirable corrosion properties in 3.5 wt % aqueous solutions of NaCl, Na_2SO_4, $NaClO_3$, and $NaNO_3$. This method provides a novel and fast process to protect the surface of magnesium alloys. Furthermore, compared with other methods for preparing superhydrophobic surfaces, this method has the advantages of simple operation, low cost, low toxicity, and convenience, and it is believed that this technique may open a novel approach to expand the applications of magnesium alloys.

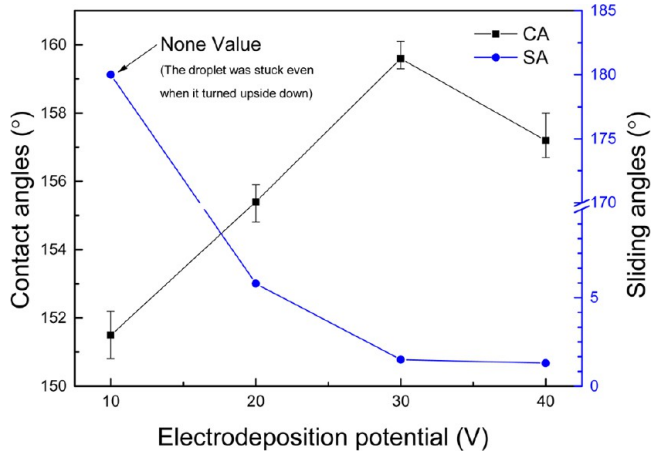

Figure 2. Variation in the water contact and sliding angles of the surfaces as functions of the electrodeposition voltage.

2. EXPERIMENTAL DETAILS

2.1. Materials and Reagents. The chemical composition of the Mg−Mn−Ce magnesium alloy was 1.5 wt % Mn, 0.3 wt % Ce, and balance Mg. The dimensions of the specimens were 30 mm × 20 mm × 4 mm. Before the electrodeposition process, the specimens were polished with a series of emery papers (up to 2000 grit), degreased ultrasonically in acetone for 10 min, and dried in air. A platinum plate (purity 99%) with dimensions of 50 mm × 30 mm × 0.5 mm was used as the anode in the electrodeposition process. All of the reagents were of analytical grade. Deionized water with a resistivity of 18.2 MΩ·cm was used in all of the experiments.

2.2. Electrodeposition Process. The electrodeposition process was performed on a direct-current power supply (Zhaoxin RXN-605D) at a constant voltage for a certain time at room temperature, where the

DOI: 10.1021/am507586u
ACS Appl. Mater. Interfaces 2015, 7, 1859−1867

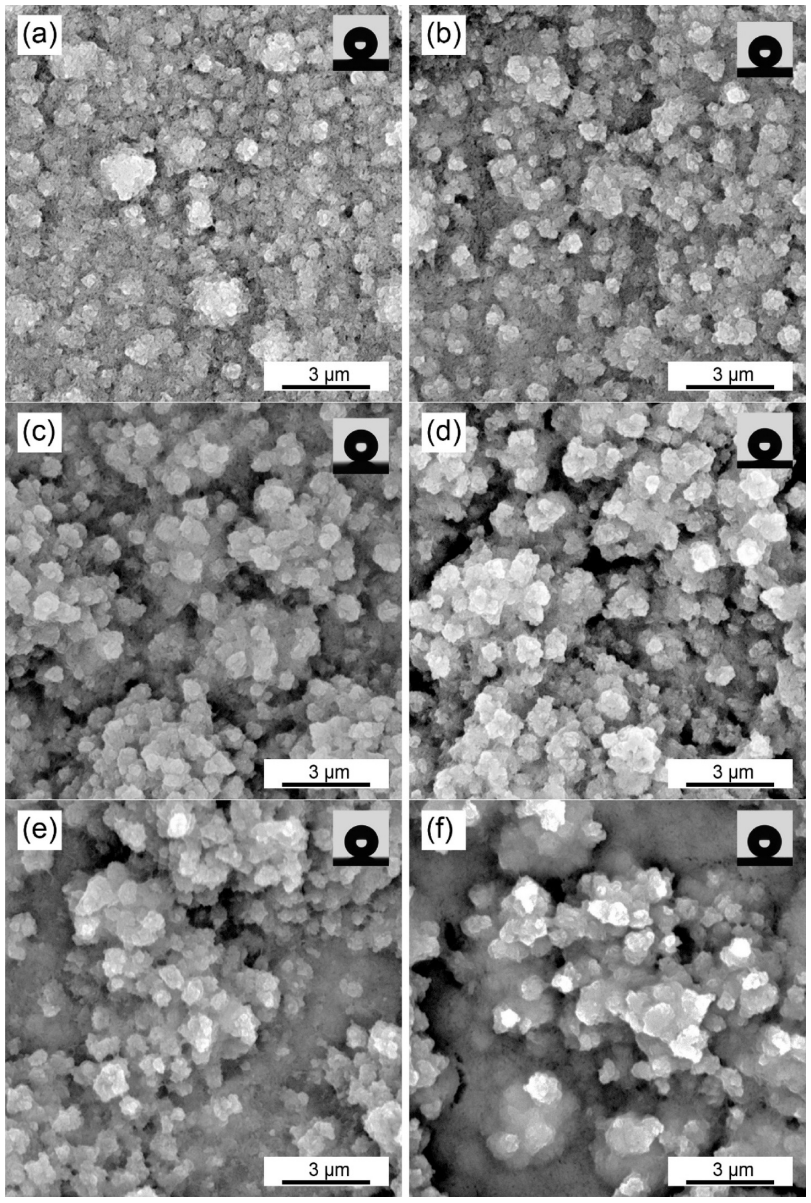

Figure 3. SEM images and (insets) water contact angles of the as-prepared superhydrophobic surfaces obtained at 30 V with different electrodeposition times: (a) 1 min, (b) 5 min, (c) 10 min, (d) 20 min, (e) 30 min, and (f) 60 min.

specimen was used as the cathode and the platinum plate mentioned above as the anode. The cathodic specimen and the anodic platinum plate were separated by a distance of 2 cm. Cerium(III) nitrate hexahydrate (0.05 M) and myristic acid (MA) (0.2 M) immersed in ethanol was used as the electrolyte solution. After deposition, the specimen was removed from the electrolyte, immediately rinsed thoroughly with ethanol, and dried under atmospheric conditions.

2.3. Characterization and Tests. The water contact angles (CAs) were measured by an optical contact angle meter (OCA35, Dataphysics) with 3 μL drops of distilled water at ambient temperature. The average value was determined by measuring the same sample at three different positions. The surface morphologies were observed by scanning electron microscopy (SEM) using a scanning electron microscope (Phenom proX, Phenom-World BV) equipped with an X-act electron microprobe for energy-dispersive X-ray spectroscopy (EDS). The chemical composition was analyzed by X-ray photoelectron spectroscopy (XPS) (AXIS Ultra, Kratos) using the C 1s peak energy (284.6 eV) as a calibrated energy standard and by Fourier-transform infrared (FT-IR) spectroscopy (VERTEX 70, Bruker).

The corrosion behaviors of the samples in 3.5 wt % aqueous solutions of NaCl, Na_2SO_4, $NaClO_3$, and $NaNO_3$ were evaluated by potentiodynamic polarization and electrochemical impedance spectroscopy (EIS) at room temperature using an electrochemical workstation (IM6ex, Zahner). A standard three-electrode system was used in the electrochemical tests, with a Ag/AgCl reference electrode, a platinum mesh as the counter electrode, and the sample with an exposed area of 1 cm^2 as the working electrode. The potentiodynamic polarization curves were measured at a scan rate of 5 mV/s. The EIS measurements were conducted over the frequency range from 100 kHz to 0.1 Hz with a sinusoidal signal amplitude of 5 mV. Before the tests, the specimens were exposed to the aqueous solution for 30 min to stabilize.

3. RESULTS AND DISCUSSION

3.1. Effect of Electrodeposition Voltage on Morphology and Wettability. Figure 1 displays SEM images of the as-prepared surface under different electrodeposition voltages for 10 min. Figure 1a shows the SEM morphology of the specimen at an electrodeposition voltage of 10 V, in which a sheetlike structure is connected into irregular porous micro/nanostructures.

DOI: 10.1021/am507586u
ACS Appl. Mater. Interfaces 2015, 7, 1859−1867

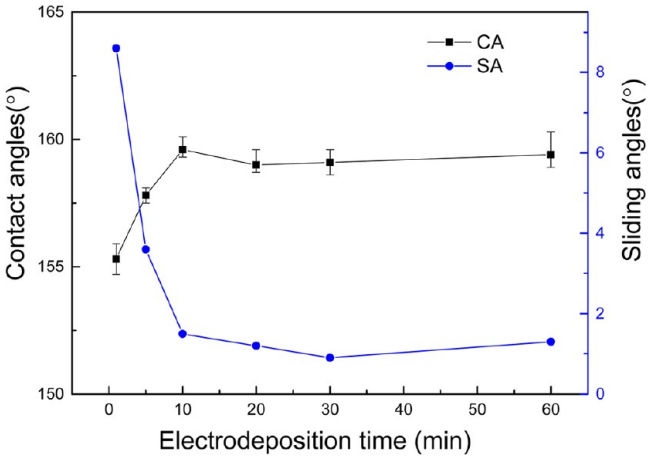

Figure 4. Variation in the water contact and sliding angles of the surfaces obtained at different electrodeposition times at a voltage of 30 V.

Figure 1b shows an SEM image of the specimen at a voltage of 20 V, in which the sheetlike structure has begun to agglomerate as papillae particles distributed randomly on the surface. As shown in Figure 1c, when the voltage was increased to 30 V, the agglomerated papillae particles were gathered to form larger papillae particles, and hierarchical micro/nanopapillae structures were constructed. At a deposition voltage of 40 V (Figure 1d), the hierarchical papillae structures were also observed, but they were not distributed as homogeneously as those shown in Figure 1c, which may be attributed to discharge and partial damage to the structure under such a high voltage.

As illustrated in Figure 1, the morphology of the surface varied with the electrodeposition voltage. The corresponding static water contact angles were measured (Figure 1insets), and the results are shown in Figure 2. The contact angle reached 151.5 ± 0.7° at a deposition voltage of 10 V. When the voltage was increased to 20 V, the contact angle was enhanced to 155.4 ± 0.6°. When the deposition voltage became 30 V, the largest contact angle of 159.6 ± 0.5° was obtained. Moreover, when the electrodeposition voltage was further increased to 40 V, the contact angle was 157.2 ± 0.8°. It is worth mentioning that except for the as-prepared surface at a voltage of 10 V, the sliding angles (SAs) of all the specimens were less than 10°, which indicates that the as-prepared surface exhibits good superhydrophobicity. As known to us, the wettability was controlled by the structure and composition of the surface. The hierarchical micro/nanoscaled papillae structure has a better ability to trap air and increase the superhydrophobicity compared with the sheetlike structure.

3.2. Effect of Electrodeposition Time on Morphology and Wettability. In order to study the effect of the electrodeposition processing time on the wettability, SEM images of the as-prepared surfaces with different electrodeposition times at an electrodeposition voltage of 30 V were obtained (Figure 3). After electrodeposition for 1 min (Figure 3a), many small papillae particles, which were composed of sheetlike structures (as mentioned above), were distributed on the surface. When the electrodeposition time was extended to 5 min (Figure 3b), the small papillae began to connect with each other and agglomerate as larger papillae. When electrodeposition time was prolonged to 10 and 20 min (Figure 3c,d), the agglomeration process continued, and obviously homogeneous hierarchical papillae structures were constructed on the surface. However, when the process time was increased to 30 and 60 min (Figure 3e,f), obviously holes were generated as a result of discharge under the long-time current on the surface.

The corresponding contact angles are plotted versus electrodeposition time in Figure 4. The static contact angles were all above 155°, and the sliding angles were all less than 10°. When the electrodeposition time was longer than 10 min, the static contact angles were all above 159° and the sliding angles were all less than 2°, which indicates that the surface exhibited good hydrophobicity under a voltage of 30 V whatever the electrodeposition time was.

3.3. Characteristics and Features of the Superhydrophobic Surface. On the basis of the analysis of the effect of electrodeposition voltage and electrodeposition time on the morphology and wettability, an electrodeposition voltage of 30 V and electrodeposition time of 10 min were chosen as the optimal parameters to fabricate the superhydrophobic surface.

3.3.1. Mechanism of the Superhydrophobicity. After the hierarchical micro/nanopapillae structures were obtained, the CA increased to 159.8° compared with 46.1° for the substrate, and the sliding angle was about 1°, indicating that the specimen exhibited good water repellency and a superhydrophobic surface was acquired. It is well-known that hierarchical micro/nanoscaled papillae structures play an important role in the wettability of a solid surface. A large amount of air can be trapped in the gaps generated in the hierarchical structure, which can lead to the larger CA and smaller SA according to the Cassie–Baxter equation:[18,25]

$$\cos\theta = f\cos\theta_0 + f - 1$$

where f is the area fraction of the water–solid interface and θ and θ_0 represent the water CAs of the micro/nanostructured and smooth surfaces, respectively. The CA of MA on a smooth surface is only about 109°.[26] Herein it was calculated that f = 0.09, demonstrating that the contact-area fraction of the water–air interface is 0.91. The large contact area between the water and air is effective in preventing the penetration of water droplets into the surface.

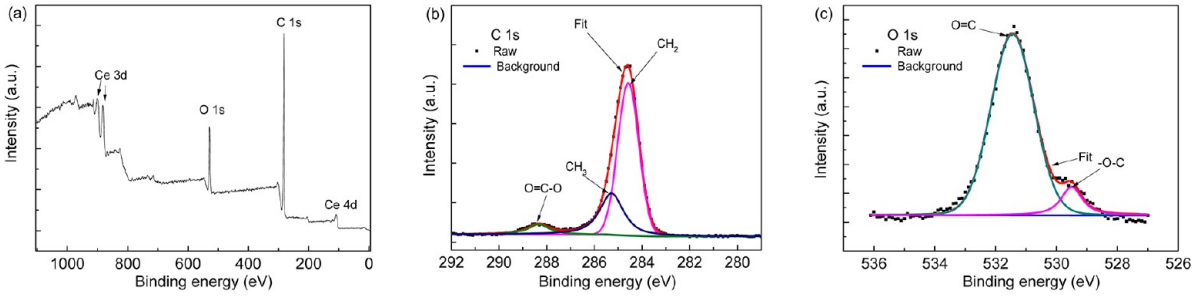

Figure 5. XPS spectra of the as-prepared superhydrophobic surface: (a) survey spectrum, (b) C 1s region, and (c) O 1s region.

DOI: 10.1021/am507586u
ACS Appl. Mater. Interfaces 2015, 7, 1859–1867

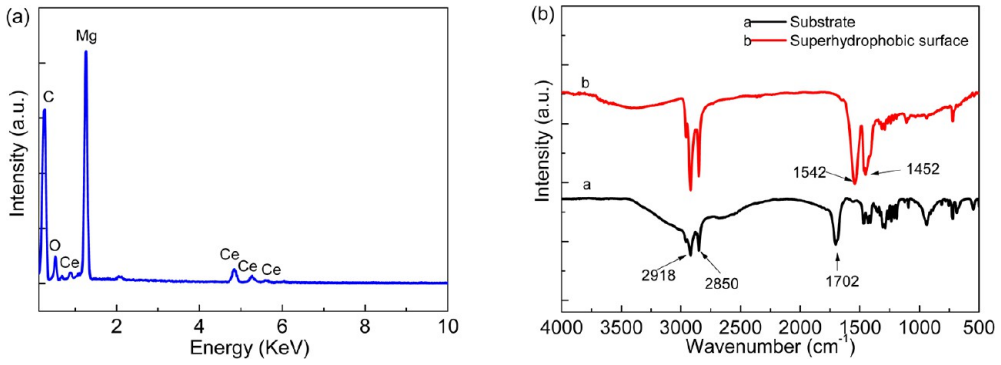

Figure 6. Chemical composition analysis of the superhydrophobic surface: (a) EDS and (b) FT-IR.

Table 1. Concentrations Determined by EDS for the As-Prepared Superhydrophobic Surface

wt %				atom %			
Mg	Ce	C	O	Mg	Ce	C	O
22.02	13.88	54.26	9.84	14.76	1.61	73.61	10.02

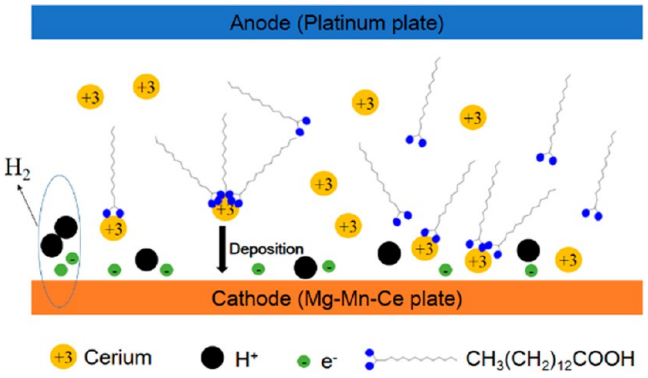

Figure 7. Schematic illustration of the electrodeposition process.

3.3.2. Formation Mechanism of the Superhydrophobic Surface. XPS, EDS, and FT-IR spectra were utilized to analyze the chemical composition of the superhydrophobic surface. Figure 5 presents the XPS survey spectrum of the as-prepared superhydrophobic surface. The presence of C, O, and Ce on the as-prepared surface can be observed in Figure 5a. Figure 5b,c shows the C 1s and O 1s decomposition-fitted curves of the XPS spectra respectively, which were investigated for further confirmation of the chemical composition of the as-prepared surface. As a result, the C 1s spectrum consists of three peaks; the peak at 284.6 eV is attributed to $-CH_2$; the peak located at 285.3 eV is assigned to $-CH_3$; and the peak located at 288.3 eV is attributed to the $-O-C{=}O$ (carboxyl) group of MA. The O 1s spectrum of the as-prepared surface shows two main peaks; the peak at a binding energy of 531.4 eV is due to the O=C bond, and the peak located at 529.5 eV can be assigned to the $-O-C$ bond. The XPS results indicate that MA was deposited onto the specimen surface.

Figure 6a shows the EDS regional analysis of the sample shown in Figures 1c and 3c, and the concentrations of elements contained in the superhydrophobic surface are listed in Table 1. It was found that the Ce/C/O atomic ratio was about 1:45.7:6.2. On the basis of the chemical valences of Ce^{3+} and $CH_3(CH_2)_{12}COO^-$ in the solution, we can deduce that cerium myristate, $Ce(CH_3(CH_2)_{12}COO)_3$ (Ce/C/O atomic ratio 1:42:6), is formed on the superhydrophobic surface. Figure 6b reveals the FT-IR spectra of pure MA and the superhydrophobic surface. In the high-frequency region of the two curves, the adsorption peaks at about 2850 and 2918 cm^{-1} are attributed to C−H asymmetric and symmetric stretching vibrations, respectively. In the low-frequency region, the peak for the carboxyl (−COO) group of MA at 1702 cm^{-1} is no longer present at the superhydrophobic surface. Two new peaks appear at 1542 and 1452 cm^{-1} that correspond to the appearance of carboxylate (cerium myristate). Consequently, the as-prepared superhydrophobic surface formed on the Mg−Mn−Ce alloy with low surface energy is cerium myristate.

Figure 7 shows a schematic illustration of the electrodeposition process. When the DC voltage is applied to the electrodes, the Ce^{3+} ions near the cathode react with MA to form cerium myristate and hydrogen ions (H^+). Meanwhile, the concentration of free H^+ ions in the solution increases, and

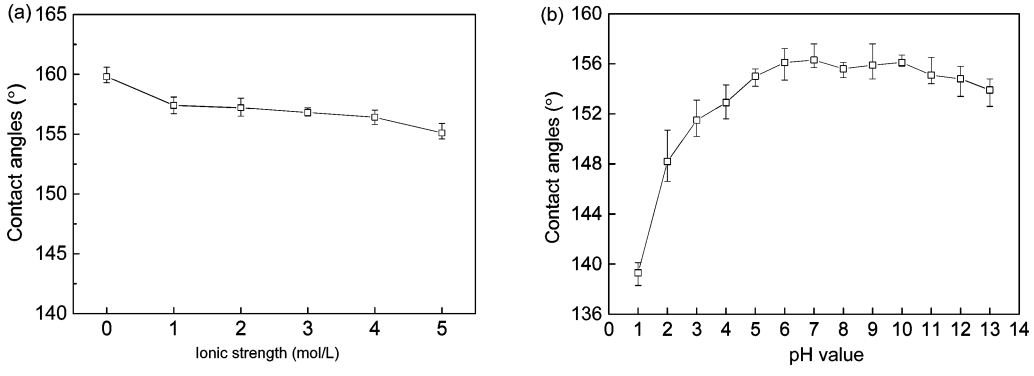

Figure 8. CA of the as-prepared superhydrophobic surface as a function of (a) ionic strength and (b) pH.

DOI: 10.1021/am507586u
ACS Appl. Mater. Interfaces 2015, 7, 1859−1867

some of them gain electrons to form H_2. The reaction equations are described as follows:[4]

$$Ce^{3+} + 3CH_3(CH_2)_{12}COOH \rightarrow Ce(CH_3(CH_2)_{12}COO)_3 + 3H^+ \quad (1)$$

$$3H^+ + 3e^- \rightarrow \frac{3}{2}H_2 \quad (2)$$

3.3.3. Chemical Stability and Mechanical Stability. Figure 8a shows the relationship between the CA and ionic strength in solutions with different concentrations of NaCl as the media on the superhydrophobic surface. It is clearly shown that the contact angles were all larger than 150° when the NaCl solution concentration varied from 0 to 5 mol/L, indicating that the superhydrophobic surface could retain its superhydrophobicity toward liquids with high salinity. Additionally, the variation of CA with pH ranging from 1 to 13 was measured. As shown in Figure 8b, all of the CAs were in the range from 150° to 157° except at pH 1 and pH 2. These results indicate that the as-prepared superhydrophobic surface shows superhydrophobicity for corrosive water under basic conditions. However, at pH 1 and pH 2, the CAs were less than 150°, which indicates that the superhydrophobicity of the surface could not bear a strongly acidic environment. This may be due to the dissolution of the $Ce(CH_3(CH_2)_{12}COO)_3$ on the Mg substrate in the strongly acidic environment. The micro/nanostructures on the surface may be destroyed as a result of the dissolution. We will try to solve this problem in future work.

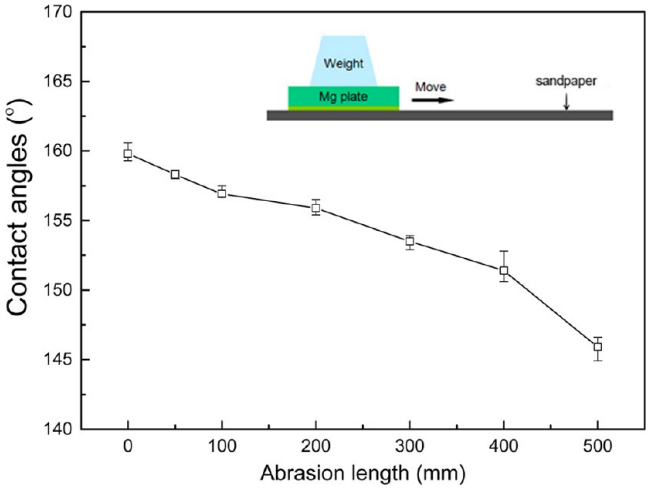

Figure 9. Schematic diagram of the abrasion test and CA of the superhydrophobic surface as a function of abrasion length.

The mechanical stability was characterized by an abrasion test, as shown in Figure 9. The superhydrophobic surface was dragged to move on 1000 grit sandpaper in one direction under a pressure of 1.3 kPa. Changes in the contact angle of the superhydrophobic surfaces were demonstrated. The results show that the as-prepared surface still maintained a CA above 150° after abrasion for 400 mm. However, after abrasion for 500 mm, the CA of the as-prepared surface decreased to 147.9 ± 1°. Despite that, the as-prepared surface showed good mechanical durability to some extent.

3.3.4. Corrosion Resistance Performance. Potentiodynamic polarization is widely used to evaluate the instantaneous corrosion rate of a tested specimen. The corrosion potential (E_{corr}) and corrosion current density (I_{corr}) parameters obtained from polarization curves directly reflect the electrochemical corrosion behavior. Generally, better corrosion resistance possesses a lower corrosion rate, which corresponds to a lower I_{corr} or a higher E_{corr}.[17,27] Figure 10 shows the potentiodynamic polarization

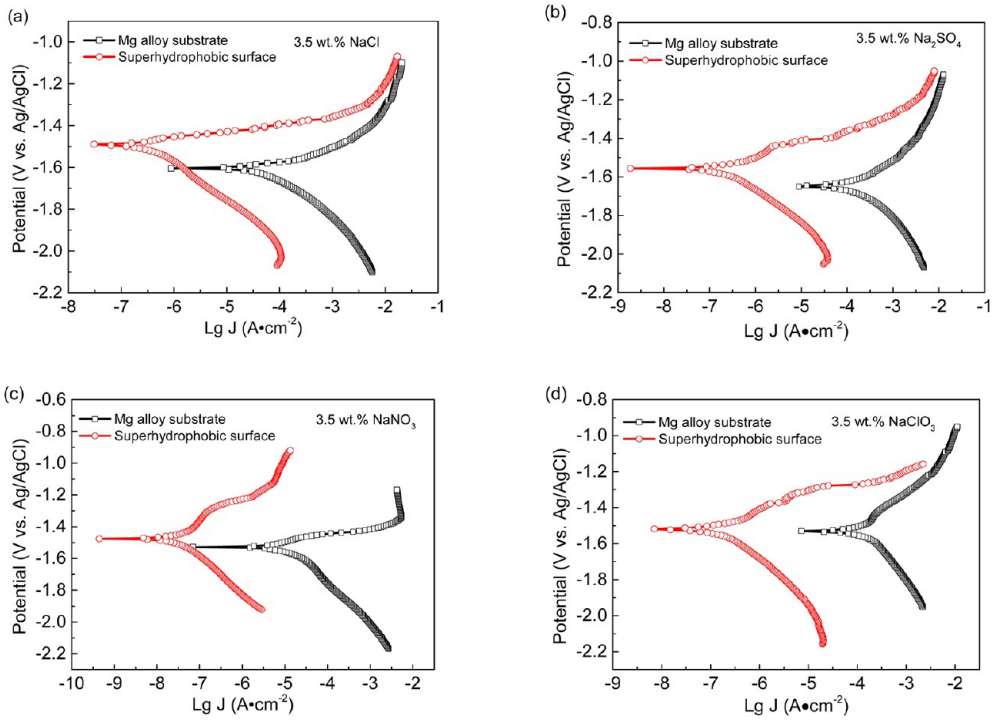

Figure 10. Potentiodynamic polarization curves of the bare and superhydrophobic surfaces in different 3.5 wt % corrosive aqueous solutions: (a) NaCl, (b) Na_2SO_4, (c) $NaNO_3$, and (d) $NaClO_3$.

DOI: 10.1021/am507586u
ACS Appl. Mater. Interfaces 2015, 7, 1859−1867

Table 2. Corrosion Potentials (E_{corr}) and Corrosion Current Densities (I_{corr}) of the Untreated and Superhydrophobic Mg Alloy Surfaces in Different Corrosive Solutions

	NaCl solution		Na_2SO_4 solution		$NaNO_3$ solution		$NaClO_3$ solution	
specimen	E_{corr} (V)	I_{corr} (A cm^{-2})	E_{corr} (V)	I_{corr} (A cm^{-2})	E_{corr} (V)	I_{corr} (A cm^{-2})	E_{corr} (V)	I_{corr} (A cm^{-2})
bare Mg surface	−1.596	2.48×10^{-5}	−1.647	1.16×10^{-4}	−1.521	4.56×10^{-6}	−1.526	6.92×10^{-5}
superhydrophobic surface	−1.489	1.42×10^{-7}	−1.564	1.08×10^{-7}	−1.476	1.48×10^{-8}	−1.513	7.82×10^{-8}

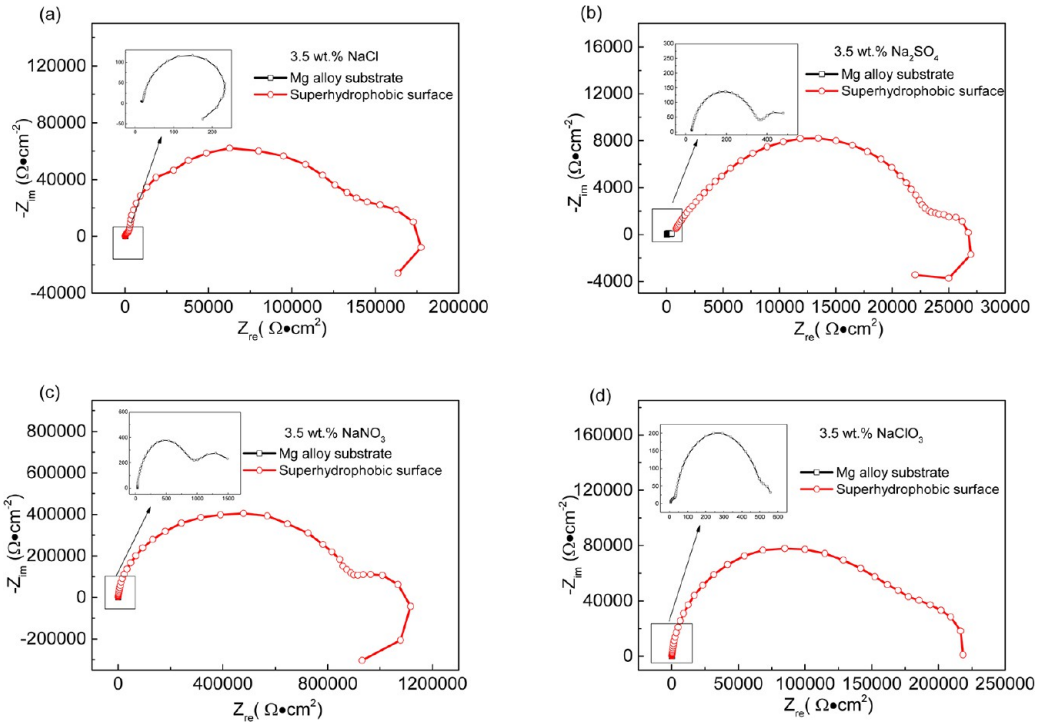

Figure 11. Nyquist plots of the bare and superhydrophobic surfaces in different 3.5 wt % corrosive aqueous solutions: (a) NaCl, (b) Na_2SO_4, (c) $NaNO_3$, and (d) $NaClO_3$.

curves for the magnesium substrate and the as-prepared superhydrophobic surface in different corrosive media, and the parameters are displayed in Table 2. It can be seen that the E_{corr} of the superhydrophobic surface in 3.5 wt % NaCl solution positively increases to −1.489 V from −1.596 V for the substrate. Accordingly, the I_{corr} in 3.5 wt % NaCl solution for the substrate is 2.48×10^{-5} A·cm^{-2}, while after superhydrophobic treatment the I_{corr} is 1.42×10^{-7} A·cm^{-2}. Compared with the value for the substrate, the I_{corr} of the superhydrophobic surface is smaller by more than 2 orders of magnitude. The increase in E_{corr} and decrease in I_{corr} suggest that the superhydrophobic surface greatly improved the corrosion resistance of the Mg−Mn−Ce alloy in NaCl solution. Similarly, in the 3.5 wt % Na_2SO_4, $NaClO_3$, and $NaNO_3$ aqueous solutions, the superhydrophobic surface also exhibited a much lower I_{corr} and a higher E_{corr}. The potentiodynamic polarization results indicate that the superhydrophobic surface has an excellent corrosion resistance in different corrosive media.

Electrochemical impedance spectroscopy is often used as a supplement to potentiodynamic polarization for a better evaluation of the corrosion behavior. Figure 11 displays the Nyquist plots of the bare magnesium alloy and the as-prepared superhydrophobic surfaces. Many researchers have found that the capacitive loop at high frequency is ascribed to the charge transfer resistance (R_{ct})[12,15,28] and that the diameter of the capacitive loop related to R_{ct} in the Nyquist plots represents the impedance of the samples. It can be clearly seen in Figure 11 that the superhydrophobic surface exhibited much higher impedance values in the 3.5 wt % aqueous solutions of NaCl, Na_2SO_4, $NaNO_3$, and $NaClO_3$, indicating that the as-prepared superhydrophobic surface has a much better corrosion resistance in the above corrosive media. It should be noted in Figure 11 that although the electrochemical behavior of the bare Mg−Mn−Ce alloy was different in the different corrosive media, the electrochemical behavior of the as-prepared superhydrophobic surface was similar in the different media. It was clearly found that the plot for superhydrophobic surface displays capacitive loops at both high and low frequencies. The high-frequency loop is related to R_{ct}, and the lower-frequency one is ascribed to the process of diffusion through the superhydrophobic surface.[4,15]

Figure 12 displays an illustration of the anticorrosion mechanism for the superhydrophobic surface in the corrosive solutions. Generally, the superhydrophobic surface with a low sliding angle is explained by the Cassie−Baxter state because the air trapped by the hierarchical structure can enhance the hydrophobicity. When the magnesium alloy substrate is immersed in the corrosive medium, the corrosive ions and water can easily contact the substrate and react with it. However, when the as-prepared superhydrophobic sample surface is immersed in the corrosive medium, the hierarchical structures are filled with air, which can effectively restrain the contact of the corrosive solution with the substrate. Therefore, the

DOI: 10.1021/am507586u
ACS Appl. Mater. Interfaces 2015, 7, 1859−1867

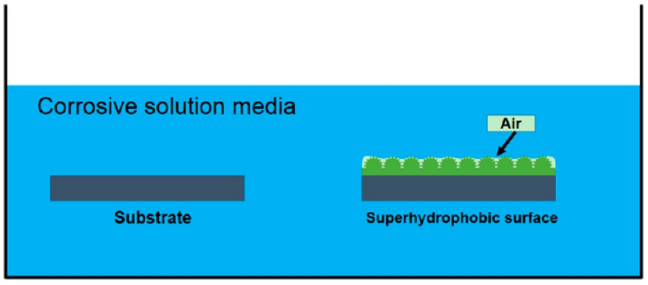

Figure 12. Interface model for the anticorrosion mechanism of the superhydrophobic surface.

corrosion rate of the superhydrophobic sample was much lower than that of the substrate in the corrosive solution medium.

4. CONCLUSIONS

In summary, a rapid one-step method was used to fabricate a superhydrophobic surface on a magnesium alloy by a simple electrodeposition process in an ethanol solution containing cerium nitrate hexahydrate and myristic acid. The time to obtain the superhydrophobic property can be as short as 1 min. The obtained surface is composed of cerium myristate with a hierarchical micro/nanoscale-particle structure and has a maximum contact angle of 159.8° and a sliding angle of less than 2°. The superhydrophobic surface shows excellent performance of corrosion resistance when immersed in corrosive aqueous solutions (3.5 wt % NaCl, Na_2SO_4, $NaClO_3$, and $NaNO_3$). Furthermore, the as-prepared surface shows good chemical stability as well as long-term durability in air. This method provides a novel, simple, and fast process to protect the surface of magnesium alloys. It is believed that this technique may open a new approach to expand the applications of magnesium alloys.

AUTHOR INFORMATION

Corresponding Author

*E-mail: zxkang@scut.edu.cn. Tel.: +86-20-87113851. Fax: +86-20-87112111.

Notes

The authors declare no competing financial interest.

ACKNOWLEDGMENTS

The authors are very grateful for the support from the National Natural Science Foundation of China (Grant 51075151) and the Key Program of the Guangdong Natural Science Foundation (Grant 10251064101000001).

REFERENCES

(1) Zuo, R. Biofilms: Strategies for Metal Corrosion Inhibition Employing Microorganisms. *Appl. Microbiol. Biotechnol.* **2007**, *76*, 1245−1253.

(2) Peng, C. W.; Chang, K. C.; Weng, C. J.; Lai, M. C.; Hsu, C. H.; Hsu, S. C.; Hsu, Y. Y.; Hung, W. I.; Wei, Y.; Yeh, J. M. Nano-casting Technique To Prepare Polyaniline Surface with Biomimetic Superhydrophobic Structures for Anticorrosion Application. *Electrochim. Acta* **2013**, *95*, 192−199.

(3) Ishizaki, T.; Masuda, Y.; Sakamoto, M. Corrosion Resistance and Durability of Superhydrophobic Surface Formed on Magnesium Alloy Coated with Nanostructured Cerium Oxide Film and Fluoroalkylsilane Molecules in Corrosive NaCl Aqueous Solution. *Langmuir* **2011**, *27*, 4780−4788.

(4) Liu, Q.; Kang, Z. One-Step Electrodeposition Process To Fabricate Superhydrophobic Surface with Improved Anticorrosion Property on Magnesium Alloy. *Mater. Lett.* **2014**, *137*, 210−213.

(5) Gu, C.; Tu, J. One-Step Fabrication of Nanostructured Ni Film with Lotus Effect from Deep Eutectic Solvent. *Langmuir* **2011**, *27*, 10132−10140.

(6) Gu, C.; Lian, J.; Li, G.; Niu, L.; Jiang, Z. Electroless Ni−P Plating on AZ91D Magnesium Alloy from a Sulfate Solution. *J. Alloys Compd.* **2005**, *391*, 104−109.

(7) Kang, Z.; Lai, X.; Sang, J.; Li, Y. Fabrication of Hydrophobic/Super-hydrophobic Nanofilms on Magnesium Alloys by Polymer Plating. *Thin Solid Films* **2011**, *520*, 800−806.

(8) Zang, D.; Zhu, R.; Wu, C.; Yu, X.; Zhang, Y. Fabrication of Stable Superhydrophobic Surface with Improved Anticorrosion Property on Magnesium Alloy. *Scr. Mater.* **2013**, *69*, 614−617.

(9) Li, W.; Kang, Z. Fabrication of Corrosion Resistant Superhydrophobic Surface with Self-Cleaning Property on Magnesium Alloy and Its Mechanical Stability. *Surf. Coat. Technol.* **2014**, *253*, 205−213.

(10) Gu, C.; Lian, J.; He, J.; Jiang, Z.; Jiang, Q. High Corrosion-Resistance Nanocrystalline Ni Coating on AZ91D Magnesium Alloy. *Surf. Coat. Technol.* **2006**, *200*, 5413−5418.

(11) Gao, R.; Liu, Q.; Wang, J.; Zhang, X.; Yang, W.; Liu, J.; Liu, L. Fabrication of Fibrous Szaibelyite with Hierarchical Structure Superhydrophobic Coating on AZ31 Magnesium Alloy for Corrosion Protection. *Chem. Eng. J.* **2014**, *241*, 352−359.

(12) Jia, J.; Fan, J.; Xu, B.; Dong, H. Microstructure and Properties of the Super-hydrophobic Films Fabricated on Magnesium Alloys. *J. Alloys Compd.* **2013**, *554*, 142−146.

(13) Khorsand, S.; Raeissi, K.; Ashrafizadeh, F. Corrosion Resistance and Long-Term Durability of Super-hydrophobic Nickel Film Prepared by Electrodeposition Process. *Appl. Surf. Sci.* **2014**, *305*, 498−505.

(14) Ishizaki, T.; Hieda, J.; Saito, N.; Saito, N.; Takai, O. Corrosion Resistance and Chemical Stability of Super-hydrophobic Film Deposited On Magnesium Alloy AZ31 by Microwave Plasma-Enhanced Chemical Vapor Deposition. *Electrochim. Acta* **2010**, *55*, 7094−7101.

(15) Wang, Y.; Wang, W.; Zhong, L.; Wang, J.; Jiang, Q.; Guo, X. Super-hydrophobic Surface on Pure Magnesium Substrate by Wet Chemical Method. *Appl. Surf. Sci.* **2010**, *256*, 3837−3840.

(16) Gnedenkov, S. V.; Egorkin, V. S.; Sinebryukhov, S. L.; Vyaliy, I. E.; Pashinin, A. S.; Emelyanenko, A. M.; Boinovich, L. B. Formation and Electrochemical Properties of the Superhydrophobic Nanocomposite Coating on PEO Pretreated Mg−Mn−Ce Magnesium Alloy. *Surf. Coat. Technol.* **2013**, *232*, 240−246.

(17) Xu, W.; Song, J.; Sun, J.; Lu, Y.; Yu, Z. Rapid Fabrication of Large-Area, Corrosion-Resistant Superhydrophobic Mg Alloy Surfaces. *ACS Appl. Mater. Interfaces* **2011**, *3*, 4404−4414.

(18) She, Z.; Li, Q.; Wang, Z.; Tan, C.; Zhou, J.; Li, L. Highly Anticorrosion, Self-Cleaning Superhydrophobic Ni−Co Surface Fabricated on AZ91D Magnesium Alloy. *Surf. Coat. Technol.* **2014**, *251*, 7−14.

(19) Liu, K.; Zhang, M.; Zhai, J.; Wang, J.; Jiang, L. Bioinspired Construction of Mg−Li Alloys Surfaces with Stable Superhydrophobicity and Improved Corrosion Resistance. *Appl. Phys. Lett.* **2008**, *92*, No. 183103.

(20) Wang, Z.; Li, Q.; She, Z.; Chen, F.; Li, L. Low-Cost and Large-Scale Fabrication Method for an Environmentally-Friendly Superhydrophobic Coating on Magnesium Alloy. *J. Mater. Chem.* **2012**, *22*, 4097−4105.

(21) Su, F.; Yao, K. Facile Fabrication of Superhydrophobic Surface with Excellent Mechanical Abrasion and Corrosion Resistance on Copper Substrate by a Novel Method. *ACS Appl. Mater. Interfaces* **2014**, *6*, 8762−8770.

(22) Liu, Y.; Yin, X.; Zhang, J.; Yu, S.; Han, Z.; Ren, L. An Electrodeposition Process for Fabrication of Biomimetic Super-hydrophobic Surface and Its Corrosion Resistance on Magnesium Alloy. *Electrochim. Acta* **2014**, *125*, 395−403.

(23) She, Z.; Li, Q.; Wang, Z.; Li, L.; Chen, F.; Zhou, J. Novel Method for Controllable Fabrication of a Superhydrophobic CuO Surface on AZ91D Magnesium Alloy. *ACS Appl. Mater. Interfaces* **2012**, *4*, 4348−4356.

DOI: 10.1021/am507586u
ACS Appl. Mater. Interfaces 2015, 7, 1859−1867

(24) She, Z.; Li, Q.; Wang, Z.; Li, L.; Chen, F.; Zhou, J. Researching the Fabrication of Anticorrosion Superhydrophobic Surface on Magnesium Alloy and Its Mechanical Stability and Durability. *Chem. Eng. J.* **2013**, *228*, 415−424.
(25) Cassie, A. B. D.; Baxter, S. Wettability of Porous Surfaces. *Trans. Faraday Soc.* **1944**, *40*, 546−550.
(26) Chen, Z.; Li, F.; Hao, L.; Chen, A.; Kong, Y. One-Step Electrodeposition Process To Fabricate Cathodic Superhydrophobic Surface. *Appl. Surf. Sci.* **2011**, *258*, 1395−1398.
(27) Wang, J.; Li, D.; Liu, Q.; Yin, X.; Zhang, Y.; Jing, X.; Zhang, M. Fabrication of Hydrophobic Surface with Hierarchical Structure on Mg Alloy and Its Corrosion Resistance. *Electrochim. Acta* **2010**, *55*, 6897−6906.
(28) Kang, Z.; Sang, J.; Shao, M.; Li, Y. Polymer Plating on AZ31 Magnesium Alloy Surface and Film Evaluation of Corrosion Property. *J. Mater. Process. Technol.* **2009**, *209*, 4590−4594.

DOI: 10.1021/am507586u
ACS Appl. Mater. Interfaces 2015, 7, 1859−1867